Inverse modeling of satellite observations shows that the wet tropics drive the 2010-2022 methane increase

Zhen Qu,[1]* Daniel J. Jacob,[2] Anthony Bloom,[3] John Worden,[3] Robert J. Parker,[4,5] Hartmut Boesch[4,5]†

[1] Department of Marine, Earth, and Atmospheric Sciences, North Carolina State University, Raleigh, NC, USA
[2] School of Engineering and Applied Science, Harvard University, Cambridge, MA, USA
[3] Jet Propulsion Laboratory, California Institute of Technology, Pasadena, CA, USA
[4] National Centre for Earth Observation, University of Leicester, Leicester, UK
[5] Earth Observation Science, School of Physics and Astronomy, University of Leicester, UK
† now at: Institute of Environmental Physics, University of Bremen FB1, Bremen, Germany

---

Abstract

Atmospheric methane concentrations rose rapidly over the past decade and surged in 2020-2022 but the causes are unclear. We find from inverse analysis of GOSAT satellite observations that global methane emissions increased from 500 to 550 Tg a^{-1} from 2010 to 2019 and surged to 570-590 Tg a^{-1} in 2020-2022. Concentrations of tropospheric OH (the main methane sink) show no long-term trend over 2010-2019, but a decrease over 2020-2022 that explains 28% of the methane surge. The methane emission increase over 2010-2022 is mainly from the wet tropics with dominant anthropogenic and wetland contributions from Africa (43% of the global emission increase), South America (18%), Equatorial Asia (18%), and India and Pakistan (12%). Emissions from the US and Russia decreased slightly over the period. The 2020-2022 emission surge is consistent with the terrestrial water storage increase due to tropical inundation in Africa and Equatorial Asia associated with La Niña conditions.

Introduction

Methane (CH_4) is the second most important anthropogenic greenhouse gas after CO_2. Its concentration has tripled in the atmosphere since preindustrial time and has contributed a 0.6°C increase in global mean surface air temperature [*Szopa et al*., 2021]. The global mean atmospheric methane concentration increased at a rate of 5 – 13 ppbv a^{-1} from 2007 to 2019 after having stayed flat at 1770-1780 ppbv during 2000-2007. 2020-2021 saw unprecedented increase at a rate of 15-18 ppbv a^{-1} [*NOAA*, 2023]. Despite extensive characterization and quantification of the global atmospheric methane budget, the drivers of these increases have remained uncertain.

Major sources of methane include fossil fuels, livestock, rice, wastewater, wetlands, and open fires [*Saunois et al*., 2020]. The dominant loss is tropospheric oxidation by the hydroxyl radical (OH). Proposed explanations for the methane rise since 2007 have included increase in oil and gas emissions [*Hausmann et al*., 2016; *Franco et al*., 2016; *Worden et al*., 2017], increase in livestock and wetland emissions [*Schaefer et al*., 2016; *Nisbet et al*., 2016; *Y. Zhang et al*., 2021; *Worden et al.*, 2023], and decrease in OH concentrations [*Turner et al.*, 2017; *Rigby et al.*, 2017]. Atmospheric ^{13}C-CH4 isotope ($\delta^{13}C_{CH4}$) trends suggest an increase in microbial methane emissions [*Nisbet et al*., 2016, 2019; *Lan et al*., 2021 a,b; *Basu et al*., 2022; *Oh et al.*, 2022]. The surge in 2020 has been attributed to wetland emissions [*Qu et al*., 2022; *Feng et al.*, 2022a; *Drinkwater et al.*, 2023] or to a decrease in OH resulting from air pollutant reductions during the COVID-19 shutdown [*Laughner et al.*, 2021; *Stevenson et al.*, 2022; *Peng et al.*, 2022]. The sustained surge in 2021-2022 has received little investigation so far.

Here, we use a global analytical inversion of GOSAT satellite observations of atmospheric methane to determine the factors driving methane changes from 2010 to 2022. GOSAT has been providing stable high-quality retrievals of atmospheric methane since 2009 [*Buchwitz et al.*, 2015; *Kuze et al.*, 2009, 2016; *Parker et al.*, 2020] and has been used extensively in global inverse analyses of the methane budget [*Monteil et al.*, 2013; *Cressot et al*., 2014; *Alexe et al.*, 2015; *Pandey et al.*, 2016; *Janardanan et al.*, 2020; *Stanevich et al.*, 2021]. The analytical inversion optimizes methane emissions to fit the GOSAT observations in a Bayesian framework with closed-form expressions of information content and straightforward generation of inversion ensembles [*Maasakkers et al.*, 2019; *Y. Zhang et al.*, 2021; *Lu et al.*, 2021; *Qu et al.*, 2021].

We perform independent Bayesian analytical inversions of GOSAT methane observations for each individual year over 2010 – 2022. For each year, the inversion optimizes a set of variables (henceforth collectively referred to as the "state vector") consisting of (1) annual mean non-wetland methane emissions in land-containing 4°×5° grid cells (1009 elements), (2) monthly wetland methane emissions in 14 subcontinental regions (168 elements), and (3) annual hemispheric methane loss frequency against oxidation by tropospheric OH (2 elements). We use the GEOS-Chem global chemical transport model with 4°×5° horizontal resolution as the forward model in the inversion to relate the state vector elements to the dry column mixing ratios (X_{CH4}) observed by GOSAT. Starting from prior estimates for all state vector elements, we produce optimized posterior estimates by drawing information from the observations following Bayes' theorem (see Methods for details). We estimate the errors in the posterior estimates for each year from the spread of a 10-member inversion ensemble with varying inversion parameters. The prior emission estimates are 2010-2019 mean values from the Global Fuel Exploitation Inventory (GFEI) version 2.0 [*Scarpelli et al.*, 2022] for oil, gas, and coal exploitation; the EDGAR v4.3.2 inventory [*Janssens-Maenhout et al.*, 2019] for other anthropogenic sources; and the nine highest-performance members of the WetCHARTs v1.3.1 wetlands inventory ensemble [*Ma et al.*, 2021] for individual months. Loss of methane from oxidation by tropospheric OH is calculated with archived 3-D climatological monthly fields of OH concentrations from a GEOS-Chem full-chemistry simulation [*Wecht et al.*, 2014] and accounts for 86% of the total atmospheric loss of methane (additional minor sinks include oxidation by Cl atoms, stratospheric oxidation, and soil uptake). The prior estimates include no 2010-2022 trends in emissions or sinks, so that all trend information is from the observations. The GEOS-Chem inversion is initialized on January 1 of each year with GOSAT observations so that subsequent discrepancies with observations reflect emissions for that year. See Methods for more details.

Results

2010-2022 global trends of methane emissions and tropospheric OH

Figure 1 (a) shows the relative changes in global mean methane concentration from 2010 to 2022 as measured by GOSAT (dry column mixing ratios X_{CH4}) and by the surface sites reporting to NOAA's Earth System Research Laboratory [*NOAA*, 2023]. The GOSAT and NOAA increasing trends are consistent. The prior GEOS-Chem simulation shows a decrease during that period because the balance between prior emissions and sinks is negative. The posterior simulation with optimized methane emissions and OH concentrations effectively corrects the trend. It does not exactly match the observed trend because we optimize 1179 independent state vector elements, which provides a wealth of information for trend attribution but leads to some smoothing with the prior estimates. But the difference is sufficiently small, particularly in the second half of the period, that we can usefully exploit the posterior estimates to interpret the observed methane trend.

Figure 1(b) shows the posterior estimates of global methane emissions and OH oxidation lifetimes in individual years. These are the two variables driving the posterior trend in global methane concentration (Figure 1(a)). The narrow spread of the inversion ensemble suggests that we can separate the role of emissions and tropospheric OH in contributing to the trend. Global methane emission increased from 500 Tg a^{-1} in 2010 to 550 Tg a^{-1} in 2019 and then more steeply to 570-590 Tg a^{-1} in 2020-2022. Anthropogenic emissions were stable at 350-380 Tg a^{-1} in 2010-2019, increased to 400-410 Tg a^{-1} in 2020-2021, and dropped back to 380 Tg a^{-1} in 2022. Wetland emissions increased from 150-180 Tg a^{-1} in 2010-2018 to 170-200 Tg a^{-1} in 2019-2022. This increase in wetland emission is consistent with the 13-26 Tg increase in 2020-2021 relative to 2000-2006 in bottom-up wetland emission model estimates [*Z. Zhang et al.*, 2023].

The posterior estimate of methane lifetime against oxidation by tropospheric OH has no significant long-term trend over 2010-2022. It has a mean value of 10.9 years, 7% longer than the prior estimate of 10.2 years and consistent with the 11.2±1.3 year estimate from the methyl chloroform proxy [*Prather et al.*, 2012]. Methane lifetime has -10%/+5% interannual variability that drives variability in the methane trend, including a 6% decrease in OH (increased lifetime) from 2019 to 2022 that would contribute to the methane surge.

Our attribution of the 2010-2019 methane concentration trend to an increase in emissions, with no significant long-term trend in OH, is consistent with previous inversions of GOSAT data for that period [*Maasakkers et al.*, 2019; *Lu et al.*, 2021; *Y. Zhang et al.*, 2021; *Yin et al.*, 2021]. The largest difference between methane sources and sinks is in 2020 and 2021 (a growth rate of 48 Tg a^{-1}), corresponding to the 15-18 ppbv a^{-1} surge in methane concentration [*NOAA*, 2023]. Tropospheric OH concentrations decreased by 3% in 2020 relative to 2019, while methane emissions increased by 7%. Several studies suggested that reduced NO_x emissions during the COVID-19 shutdown in 2020 decreased tropospheric OH [*Laughner et al.*, 2021; *Stevenson et al.*, 2022; *Peng et al.*, 2022] but we find that this is within OH interannual variability over the 2010-2022 record. The methane surge also extended into 2021, which we explain by sustained high emissions. The global methane increase slows down by 17% in 2022 [*NOAA*, 2023] because of decreasing anthropogenic methane emissions offsetting a decrease in OH.

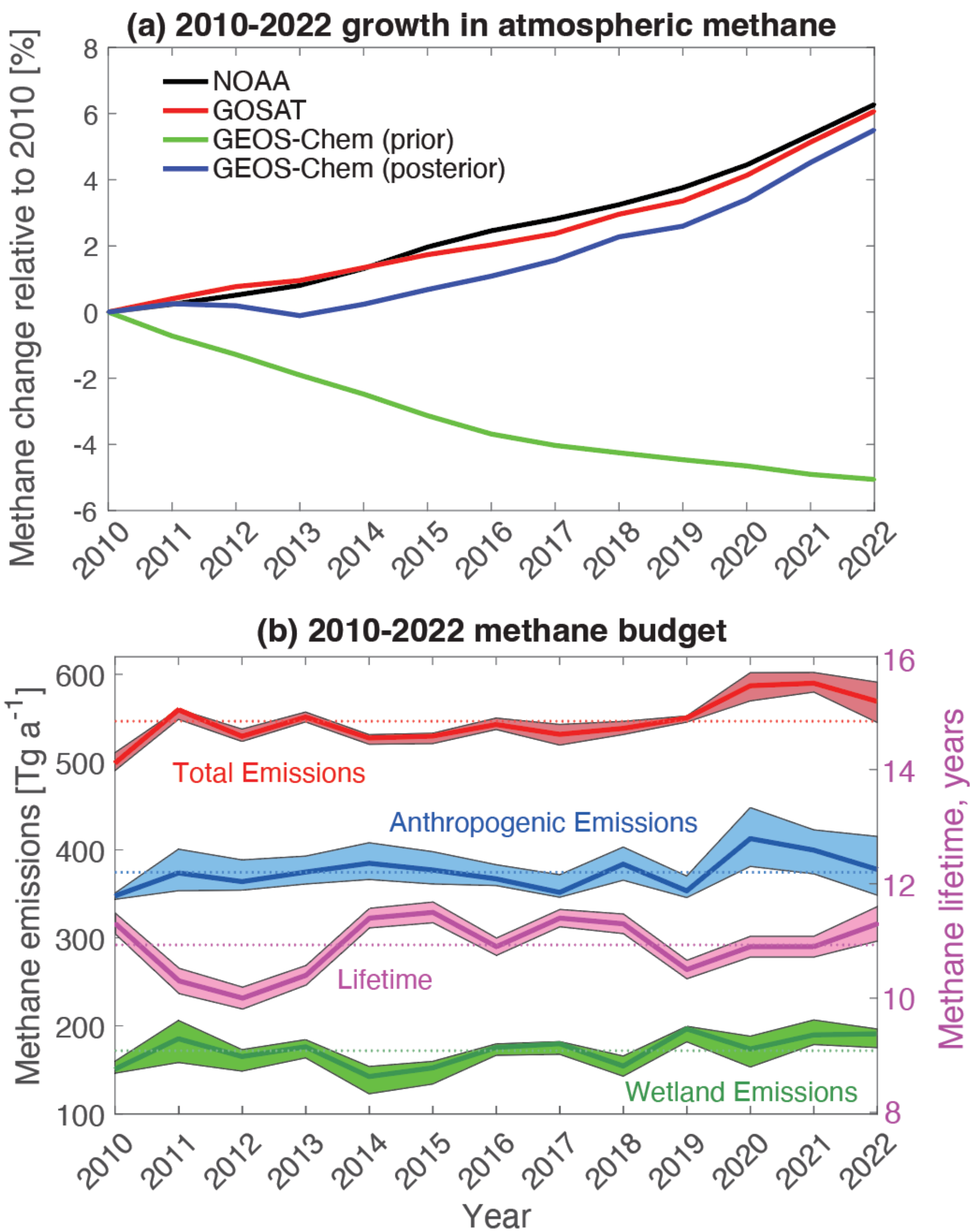

Figure 1. (a) 2010-2022 trends in global annual mean methane concentrations, expressed as changes relative to 2010. Results are shown for surface methane concentrations as reported by the Global Monitoring Division of NOAA's Earth System Research Laboratory [NOAA, 2023], dry methane column mixing ratios (X_{CH4}) measured by the GOSAT satellite instrument, and GEOS-Chem simulations of X_{CH4} using prior and posterior estimates of methane emissions and OH concentrations. (b) Posterior estimates of 2010-2022 trends in global methane emissions and lifetime against oxidation by tropospheric OH. Thick lines show results from our base inversion and shaded areas show the spread of the 10-member inversion ensemble with different inversion parameters (see Methods for details). The thin dotted lines are mean 2010-2022 values.

2010-2022 regional trends of methane emissions

Figure 2(a) shows the global distribution of the methane emission growth rates over 2010-2022 as linear regressions on the posterior estimates. The global rate of increase over that period is 5 Tg a^{-2}. The largest increases are in Africa (3 Tg a^{-2}), mostly in the central region of the continent with high wetland and livestock emissions. We also find increasing trends in Equatorial Asia (1.0 Tg a^{-2}), South America (1.0 Tg a^{-2}), India and Pakistan (0.8 Tg a^{-2}), and the Middle East (0.3 Tg a^{-2}). We find decreasing emissions in the US (-0.3 Tg a^{-2}) and Russia (-0.2 Tg a^{-2}). China (0.09 Tg a^{-2}) shows opposite emission trends over the North China Plain (increase) and South China (decrease), consistent with a shift in coal mining activity from south to north [*Y. Zhang et al.*, 2022].

Figure 2(b) shows that Africa accounts for 43% of the total emission increase from 2010 to 2022, 34% of the global anthropogenic emission increase, and 53% of the global wetland emission increase. The inversion can separate the 2010-2022 changes in anthropogenic and wetland emissions in Africa with moderate error correlations of $R = -0.6$ (see Equation 3 in the Methods). Other drivers of the global methane increase over 2010-2022 include South America (18% of the global total emission increase, 16% anthropogenic, 20% wetland, $R = -0.6$), Equatorial Asia (18% total, 9% anthropogenic, 22% wetland, $R = -0.5$), India and Pakistan (12% total, 17% anthropogenic, 2% wetland, $R = -0.5$), and the Middle East (6% total, 9% anthropogenic, 1% wetland, $R = -0.5$).

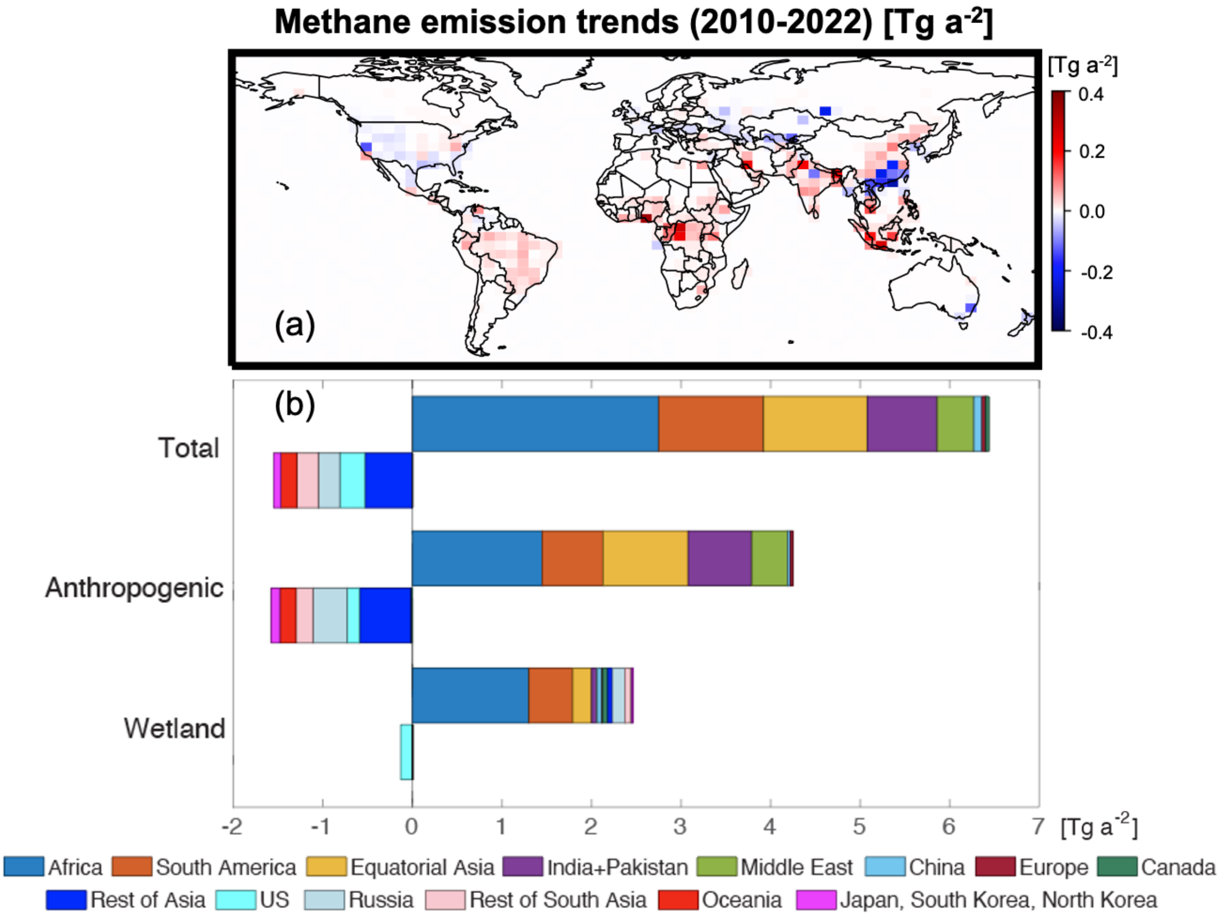

Figure 2. (a) Methane emission trends from inversion of GOSAT observations for 2010-2022. Values for each 4°×5° grid cell are fit by linear regression to the posterior emissions for individual years. (b) Emission growth rates by region for 2010-2022.

Figure 3 shows 2010-2022 emission trends for the four regions driving the global increase. 49% of the 2020-2022 surge is driven by Africa (Figure S1). Our inversion indicates a total (anthropogenic + wetland) emission increase in Africa of 20 Tg a^{-1} from 2019 to 2021-2022, comparable with the 9-year increase of 23 Tg a^{-1} from 2010 to 2019. Anthropogenic emissions in Africa have been increasing steadily over 2010-2022. This may be explained by rapid growth in livestock [*Y. Zhang et al.*, 2021; *Worden et al.*, 2023] and rice cultivation [*Chen et al.*, 2023]. Wetland emission increase in Africa has accelerated, from 3 Tg a^{-1} over 2010-2017 to 14 Tg a^{-1} over 2017-2022. Regions with the largest emission increase in Figure 2 (a) (East Africa, the Democratic Republic of the Congo, and Nigeria) represent 78% of wetland methane sources in Africa [*Ma et al.*, 2021]. Previous inverse studies of satellite methane data have pointed to an increase in African wetland emissions driven by increased inundation [*Lunt et al.*, 2021; *Feng et al.*, 2022a, b; *Qu et al.*, 2022]. Africa wetland methane emission trends are also consistent with observed terrestrial water storage trends from the Gravity Recovery and Climate Experiment satellites (GRACE and GRACE/FO; Figure S2), which provides a strong proxy for anaerobic methane production processes in wetland ecosystems [*Bloom et al.*, 2010, 2012].

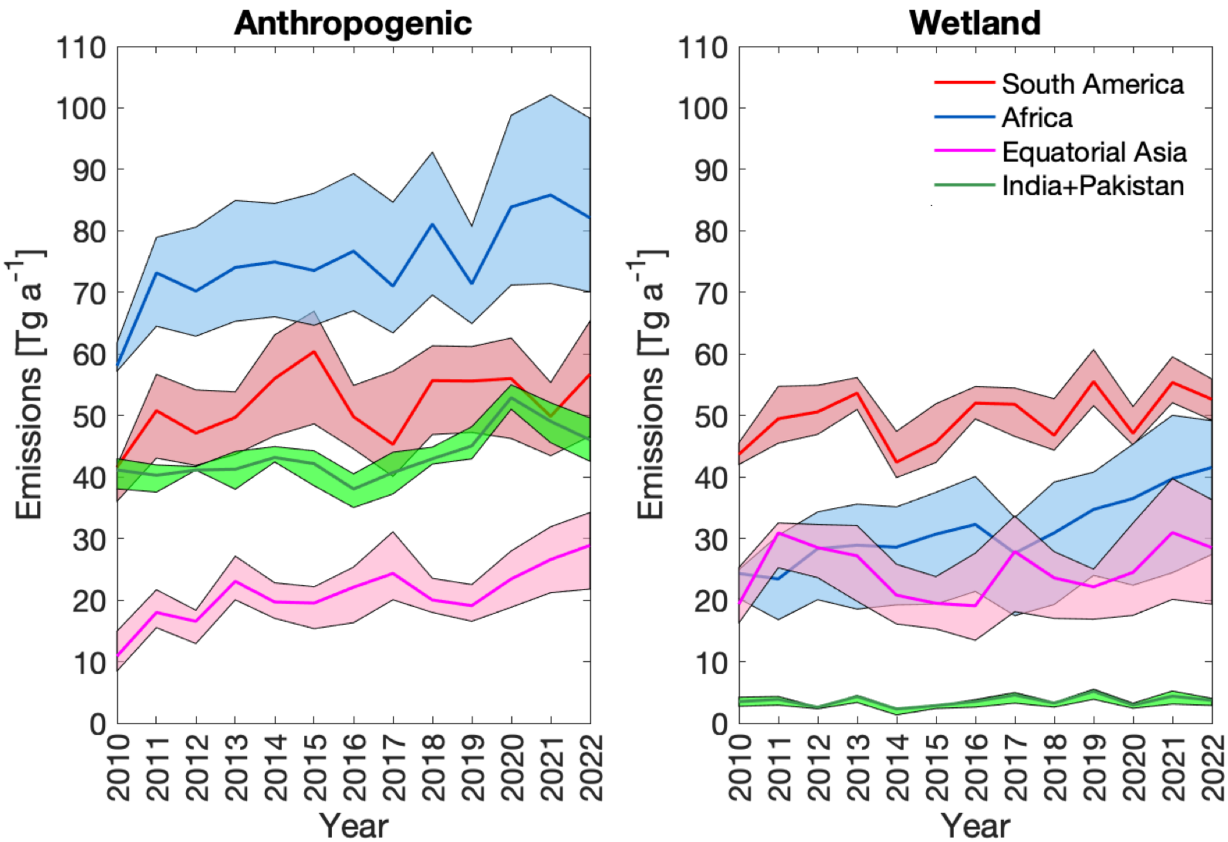

Figure 3. Regional trends of methane emissions informed by GOSAT for 2010-2022. Results are shown for the four regions driving most of the global emission increase. Lines show results from our base inversion and shaded areas show the spread of the 10-member inversion ensemble with different inversion parameters.

Equatorial Asia accounts for 41% of the methane emission surge in 2020-2022. Wetland emissions contribute to 50-65% of methane sources in this region according to our posterior estimates and have increased by 5 Tg a^{-1} (47% of the anthropogenic + wetland emission increase) from 2010-2019 to 2019-2022. Similarly to the Africa wetland regions, we find a correlated trends in GRACE and GRACE/FO observed terrestrial water storage with peaks in 2011-2012, 2017, and 2021 that are consistent with wetland methane emissions (Figure S2). In 2020 and 2021, Equatorial Asia witnessed the highest precipitation over the past decade accompanied by devastating inundations [*Hermawan et al.*, 2022; *World Bank*, 2023a, b]. The bottom-up WetCHARTs methane emissions also show a 16% increase in wetland methane emissions in Equatorial Asia from 2019 to 2020. Anthropogenic emissions steadily increased over 2010-2019 with acceleration over 2020-2022. Rice cultivation is the largest contributor to the rise of anthropogenic emissions from 2010-2019 to 2020-2022 in Equatorial Asia (30%), followed by waste (15%), oil and gas (10%), and livestock (8%). Increasing rice emissions is consistent with the increase in inundation [*Jain et al.*, 2000].

India and Pakistan show no trend in methane emissions over 2010-2019 but an 8 Tg a^{-1} surge in 2020 making that region an important contributor to the global methane surge. Posterior estimates show that livestock (50%), rice cultivation (25%), and waste (13%) are the drivers of the 2020 surge. Livestock and waste have been driving the 2009-2018 methane emissions in this region [*Worden et al.*, 2023]. Emission increase from rice cultivation may again be driven by its sensitivity to inundation. Variability in precipitation is a key factor governing rice emissions in India and Indonesia [*B. Zhang et al.*, 2016]. The 2019-2021 precipitations in India were the highest of the past decade [*Statista*, 2023], leading to floods across the country in 2020 [*Gaon Connection*, 2020;

Reliefweb, 2020]. Pakistan experienced its largest precipitation over the past decade in 2020, including heavy flooding and stagnant water in Sindh, a major rice cultivation area [*USDA*, 2023; *Dartmouth Flood Observatory*, 2020].

The heavy precipitation in these wetland and rice cultivation regions is likely associated with the La Niña conditions from 2020 to early 2023. El Nino-Southern Oscillation (ENSO) can explain much of the interannual variation of tropical wetland methane emissions [*Hodson et al.*, 2011; *Zhu et al.*, 2017; *Z. Zhang et al.*, 2018]. *Hodson et al.* [2011] analyzed the correlation between their wetland methane emission model and the ENSO index and found that La Niña events over 1950–2005 led to maximum and mean increases of 14 Tg a^{-1} and 8 Tg a^{-1} of global wetland methane emissions compared to the 1950-2005 mean value. These increases are smaller than our posterior estimate of a 20 Tg a^{-1} global increase in wetland emissions from 2010-2018 to 2019-2022. *Hodson et al.* [2011] also found that the tropics (44%) and northern temperate regions (27%) are the largest contributors to the global wetland interannual variability, whereas boreal wetland only accounts for 12%, consistent with our results.

South America is the largest contributor to the global methane emission increases prior to 2020 (26 Tg a^{-1} total increase from 2010 to 2019) but does not make a specific contribution to the 2020-2022 methane surge. Livestock is the largest anthropogenic methane source in that region (58%). The pattern of growth in Figure 2 is consistent with livestock inventories [*Chang et al.*, 2019; *Crippa et al.*, 2019; *Janssens-Maenhout et al.*, 2019; *FAOSTAT*, 2023] and previous inversions [*Y. Zhang et al.*, 2021]. The increases in wetland emissions are mainly from Amazon and north Peru.

Discussion

In summary, we find from the inversion of 2010-2022 GOSAT satellite data for individual years that global methane emission increased from 500 Tg a^{-1} to 550 Tg a^{-1} over 2010-2019 followed by a surge to 570-590 Tg a^{-1} in 2020-2022. The methane sink from oxidation by tropospheric OH does not contribute to the 2010-2019 trend, but decreasing OH contributes 28% of the observed methane surge in 2020-2022. The largest growth rate in emissions over the 2010-2022 period was from Africa (3 Tg a^{-2}, accounting for 43% of the global emission increase), followed by South America (1.0 Tg a^{-2}, 18%), Equatorial Asia (1.0 Tg a^{-2}, 18%), and India and Pakistan (0.8 Tg a^{-2}, 12%). Emissions in China, the US, and Russia were relatively flat. The emission surge in 2020-2022 is mostly from Africa (49% of the surge) and Equatorial Asia (41%). We attribute the surge mainly to emission increases from tropical wetlands and rice cultivation as a result of inundation associated with La Niña conditions. One possible explanation for such an emission increase is the precipitation changes associated with climate change [*Putnam and Broecker*, 2017; *Y. Zhang and Fueglistaler*, 2019]. Improved observations of wetland methane emissions [*Bloom et al.*, 2016] and process-based attribution of methane responses to climate change [e.g. *Ma et al.*, 2023] would help quantitatively resolve the role of changing precipitation patterns on tropical wetland ecosystems.

Materials and Methods

We use GOSAT 2010-2021 methane dry column mixing ratios (X_{CH4}) from the University of Leicester proxy product version 9.0 [*Parker and Boesch*, 2020]. GOSAT is in a polar sun-synchronous low-Earth orbit. X_{CH4} is retrieved using solar backscatter in the 1.65 μm shortwave infrared absorption band. We include retrievals over land and glint retrievals over the ocean but exclude data poleward of 60° because of the seasonal sampling bias, extensive cloudiness, and greater sensitivity to variability in the stratosphere. We filter out low-quality retrievals using "xch4_quality_flag" = 0.

We use the GEOS-Chem chemical transport model version 12.5.0 (10.5281/zenodo.3403111) at 4°×5° grid resolution to relate methane emissions and OH concentrations to X_{CH4} using the averaging kernel and prior vertical profiles in the GOSAT retrieval. GEOS-Chem is driven by the Modern-Era Retrospective analysis for Research and Applications, Version 2 (MERRA-2) meteorological fields from the NASA Global Modeling and Assimilation Office (GMAO), which use consistent model physics and data assimilation for 2010-2022. The methane simulation in GEOS-Chem is described in *Wecht et al.* [2014]. Loss of methane from oxidation by tropospheric OH is calculated with archived 3-D climatological monthly fields of OH concentrations from a full-chemistry simulation [*Wecht et al*., 2014]. Initial concentrations of methane on January 1 of each year are adjusted to match GOSAT X_{CH4} with a globally uniform scaling factor calculated using the ratio of observed and simulated X_{CH4} averaged from Jan 1 to Jan 10. This adjustment is not applied to the results of Figure 1, which shows the 2010-2022 trends of GEOS-Chem with prior and posterior budget terms in free-running simulations.

We use the same anthropogenic and wetland emissions as prior estimates for all years in the 2010-2022 period. Anthropogenic emissions are 2010-2019 means from the Global Fuel Exploitation Inventory (GFEI) version 2.0 [*Scarpelli et al.*, 2022] for oil, gas, and coal, and from the global EDGAR v4.3.2 inventory [*Janssens-Maenhout et al.*, 2019] for other sources. Emissions for the contiguous US are from the gridded version of the US Environmental Protection Agency (EPA) greenhouse gas inventory [*Maasakkers et al.*, 2016]. The seasonality of rice emissions from *B. Zhang et al.* [2016] and of manure emissions from *Maasakkers et al.* [2016] are applied locally to the EDGAR annual totals. We use monthly wetland emissions from the nine highest-performance members of the WetCHARTs v1.3.1 inventory ensemble [*Ma et al.*, 2021]. Monthly open fire emissions averaged over 2010-2019 are from the Global Fire Emissions Database version 4 (GFED4) [*van der Werf et al.*, 2017]. Termite emissions are from *Fung et al.* [1991]. Geological seepage emissions are from *Etiope et al.* [2019] and are scaled to a global magnitude of 2 Tg a^{-1} based on *Hmiel et al.* [2020].

The loss of methane from reaction with tropospheric OH has a corresponding methane lifetime of 10.2 years in the prior simulation. We also use archived Cl concentration fields from *Wang et al.* [2019] for methane oxidation by tropospheric Cl atoms, 2-D monthly loss frequencies from the NASA Global Modeling Initiative model [*Murray et al.*, 2012] for stratospheric oxidation, and the Methanotrophy Model [*Murguia-Flores et al.*, 2018] for methane soil uptake.

We use water storage data from the GRACE and GRACE/FO Mascon version RL06.2 [*Save et al.*, 2016; *Save*, 2020], with all recommended corrections applied. Ocean water storage anomalies were removed from regionally averaged GRACE time series over Equatorial Asia and Africa.

Atmospheric Inverse Analysis

The state vector $\boldsymbol{x}$ of the inversion consists of 1179 elements for each year, including (1) annual mean non-wetland methane emissions for land-containing 4°×5° grid cells (1009 elements), (2) monthly wetland methane emissions for 14 subcontinental regions (168 elements), and (3) annual hemispheric methane loss frequency against oxidation by tropospheric OH (2 elements). For each year's inversion, we perturb each of the state vector elements in 1179 GEOS-Chem simulations to construct the full Jacobian matrix $\mathbf{K}$, which describes the sensitivity of the methane observations to the state vector as simulated by GEOS-Chem. The posterior estimate with Gaussian error statistics is obtained by minimizing the scalar cost function $J(\boldsymbol{x})$:

$$J(\boldsymbol{x}) = (\boldsymbol{x} - \boldsymbol{x}_a)^T \mathbf{S_a}^{-1} (\boldsymbol{x} - \boldsymbol{x}_a) + \gamma (\boldsymbol{y} - \mathbf{K}\boldsymbol{x})^T \mathbf{S_o}^{-1} (\boldsymbol{y} - \mathbf{K}\boldsymbol{x}), \quad (1)$$

where $\boldsymbol{x}_a$ is the prior estimate of the state vector, $\mathbf{S_a}$ is the prior error covariance matrix, $\mathbf{S_o}$ is the observational error covariance matrix assumed to be diagonal, and γ is a regularization parameter that accounts for the effect of unresolved correlation in the observational error. We construct $\mathbf{S_a}$, $\mathbf{S_o}$, and γ following *Qu et al.* [2022] and *Y. Zhang et al.* [2021]. By using the same prior estimate for individual years (as opposed to a Kalman filter using the posterior estimate from the previous year), we ensure that observations from each year have equal weight in the inversion and we make no assumption of trend persistence from one year to the next.

The best posterior estimate is given by [*Rodgers*, 2000]:

$$\hat{\boldsymbol{x}} = \boldsymbol{x}_a + \left(\gamma \mathbf{K}^T \mathbf{S_o}^{-1} \mathbf{K} + \mathbf{S_a}^{-1}\right)^{-1} \gamma \mathbf{K}^T \mathbf{S_o}^{-1} (\boldsymbol{y} - \mathbf{K}\boldsymbol{x}_a). \quad (2)$$

with posterior error covariance matrix $\hat{\mathbf{S}}$:

$$\hat{\mathbf{S}} = (\gamma \mathbf{K}^T \mathbf{S_o}^{-1} \mathbf{K} + \mathbf{S_a}^{-1})^{-1}. \quad (3)$$

This expression for the posterior error covariance matrix assumes that the inversion parameters are correct but there is also uncertainty associated with those. These parameters in the base inversion include 50% error standard deviation for anthropogenic emissions on the $4^{o}\times5^{o}$ grid with no off-diagonal correlations, 50% error standard deviation for wetland emissions with off-diagonal correlations calculated from the WetCHARTs ensemble [*Bloom et al.*, 2017; *Y. Zhang et al.*, 2021], 10% error standard deviation for hemispheric annual OH concentrations, and $\gamma = 0.1$ to match the expected chi-squared value for the contribution of the prior estimate terms to the posterior cost function [*Lu et al.*, 2021]. As an alternative approach to estimate errors, we conducted inversion ensembles for each year varying parameters from our base inversion one at a time, including prior error standard deviations for anthropogenic emissions (20%, 70%), wetland emissions (20%, 70%), and hemispheric OH concentrations (5%, 20%), and regularization parameters ($\gamma = 0.05$, 0.5, and 1). This results in a 10-member inversion ensemble including the base inversion. The spread of results for that ensemble is larger than the posterior error standard deviation and we use it as a more conservative error estimate on our inversion results [*Qu et al.*, 2022; *Chen et al.*, 2022].

References

Alexe, M., Bergamaschi, P., Segers, A., Detmers, R., Butz, A., Hasekamp, O., et al. (2015). Inverse modelling of CH4 emissions for 2010–2011 using different satellite retrieval products from GOSAT and SCIAMACHY. *Atmos. Chem. Phys., 15*(1), 113-133. https://acp.copernicus.org/articles/15/113/2015/

Basu, S., Lan, X., Dlugokencky, E., Michel, S., Schwietzke, S., Miller, J. B., et al. (2022). Estimating emissions of methane consistent with atmospheric measurements of methane and δ13C of methane. *Atmos. Chem. Phys., 22*(23), 15351-15377. https://acp.copernicus.org/articles/22/15351/2022/

Bloom, A. A., Lauvaux, T., Worden, J., Yadav, V., Duren, R., Sander, S. P., and Schimel, D. S. (2016). What are the greenhouse gas observing system requirements for reducing fundamental biogeochemical process uncertainty? Amazon wetland CH4 emissions as a case study. *Atmos. Chem. Phys., 16*, 15199-15218. https://acp.copernicus.org/articles/16/15199/2016

Bloom, A. A., Palmer, P. I., Fraser, A., Reay, D. S., & Frankenberg, C. (2010). Large-Scale Controls of Methanogenesis Inferred from Methane and Gravity Spaceborne Data. *Science, 327*(5963), 322-325. https://www.science.org/doi/abs/10.1126/science.1175176

Bloom, A. A., Palmer, P. I., Fraser, A., & Reay, D. S. (2012). Seasonal variability of tropical wetland CH4 emissions: the role of the methanogen-available carbon pool. *Biogeosciences, 9*(8), 2821-2830. https://bg.copernicus.org/articles/9/2821/2012/

Bloom, A. A., Bowman, K. W., Lee, M., Turner, A. J., Schroeder, R., Worden, J. R., et al. (2017). A global wetland methane emissions and uncertainty dataset for atmospheric chemical transport models (WetCHARTs version 1.0). *Geosci. Model Dev., 10*(6), 2141-2156. https://gmd.copernicus.org/articles/10/2141/2017/

Buchwitz, M., Reuter, M., Schneising, O., Boesch, H., Guerlet, S., Dils, B., et al. (2015). The Greenhouse Gas Climate Change Initiative (GHG-CCI): Comparison and quality assessment of near-surface-sensitive satellite-derived CO2 and CH4 global data sets. *Remote Sensing of Environment, 162*, 344-362. http://www.sciencedirect.com/science/article/pii/S0034425713003520

Chang, J., Peng, S., Ciais, P., Saunois, M., Dangal, S. R. S., Herrero, M., et al. (2019). Revisiting enteric methane emissions from domestic ruminants and their δ(13)C(CH4) source signature. *Nat Commun, 10*(1), 3420.

Chen, Z., Jacob, D. J., Nesser, H., Sulprizio, M. P., Lorente, A., Varon, D. J., et al. (2022). Methane emissions from China: a high-resolution inversion of TROPOMI satellite observations. *Atmos. Chem. Phys., 22*(16), 10809-10826. https://acp.copernicus.org/articles/22/10809/2022/

Chen, Z., N., Balasus, H., Lin, H., Nesser & D. J. Jacob (2023). African rice cultivation linked to rising methane. arXiv:2307.11232. https://doi.org/10.48550/arXiv.2307.11232

Cressot, C., Chevallier, F., Bousquet, P., Crevoisier, C., Dlugokencky, E. J., Fortems-Cheiney, A., et al. (2014). On the consistency between global and regional methane emissions inferred from SCIAMACHY, TANSO-FTS, IASI and surface measurements. *Atmos. Chem. Phys., 14*(2), 577-592. https://acp.copernicus.org/articles/14/577/2014/

Crippa, M., Oreggioni, G., Guizzardi, D., Muntean, M., Schaaf, E., Lo Vullo, E., Solazzo, E., Monforti-Ferrario, F., Olivier, J.G.J., Vignati, E. (2019). Fossil CO2 and GHG emissions of all world countries - 2019 Report, EUR 29849 EN, Publications Office of the European Union, Luxembourg, 2019, ISBN 978-92-76-11100-9. https://doi.org/10.2760/687800.

Crippa, M., Solazzo, E., Huang, G., Guizzardi, D., Koffi, E., Muntean, M., et al. (2020). High resolution temporal profiles in the Emissions Database for Global Atmospheric Research. *Scientific Data, 7*(1), 121. https://doi.org/10.1038/s41597-020-0462-2

Dartmouth Flood Observatory (2020), DFO Flood Event: 2020-Pakistan-4966, available at: https://floodobservatory.colorado.edu/Events/4966/2020Pakistan4966.html, last access: Nov 19, 2023.

Drinkwater, A., Palmer, P. I., Feng, L., Arnold, T., Lan, X., Michel, S. E., et al. (2023). Atmospheric data support a multi-decadal shift in the global methane budget towards natural tropical emissions. *Atmos. Chem. Phys., 23*(14), 8429-8452. https://acp.copernicus.org/articles/23/8429/2023/

Etiope, G., Ciotoli, G., Schwietzke, S., & Schoell, M. (2019). Gridded maps of geological methane emissions and their isotopic signature. *Earth Syst. Sci. Data, 11*(1), 1-22. https://essd.copernicus.org/articles/11/1/2019/

FAOSTAT (2023). Online Statistical Service (Food and Agriculture Organization, FAO): available at: http://faostat3.fao.org, last access: Nov 19, 2023.

Feng, L., Palmer, P. I., Parker, R. J., Lunt, M. F., & Boesch, H. (2022a). Methane emissions responsible for record-breaking atmospheric methane growth rates in 2020 and 2021. *Atmos. Chem. Phys. Discuss., 2022*, 1-23. https://acp.copernicus.org/preprints/acp-2022-425/

Feng, L., Palmer, P. I., Zhu, S., Parker, R. J., & Liu, Y. (2022b). Tropical methane emissions explain large fraction of recent changes in global atmospheric methane growth rate. *Nature Communications, 13*(1), 1378. https://doi.org/10.1038/s41467-022-28989-z

Franco, B., Mahieu, E., Emmons, L. K., Tzompa-Sosa, Z. A., Fischer, E. V., Sudo, K., et al. (2016). Evaluating ethane and methane emissions associated with the development of oil and natural gas extraction in North America. *Environmental Research Letters, 11*(4), 044010. https://dx.doi.org/10.1088/1748-9326/11/4/044010

Fung, I., John, J., Lerner, J., Matthews, E., Prather, M., Steele, L. P., & Fraser, P. J. (1991). Three-dimensional model synthesis of the global methane cycle. *Journal of Geophysical Research: Atmospheres, 96*(D7), 13033-13065. https://agupubs.onlinelibrary.wiley.com/doi/abs/10.1029/91JD01247

Gaon Connection (2020). Floods 2020: The need for critical engagement with floods in India, available at: https://en.gaonconnection.com/floods-2020-the-need-for-critical-engagement-with-floods-in-india/, last access: Nov 19, 2023.

Hausmann, P., Sussmann, R., & Smale, D. (2016). Contribution of oil and natural gas production to renewed increase in atmospheric methane (2007–2014): top–down estimate from ethane and methane column observations. *Atmos. Chem. Phys., 16*(5), 3227-3244. https://acp.copernicus.org/articles/16/3227/2016/

Hermawan, E., Lubis, S. W., Harjana, T., Purwaningsih, A., Risyanto, R., Ridho, A., et al. (2022). Large-Scale Meteorological Drivers of the Extreme Precipitation Event and Devastating Floods of Early-February 2021 in Semarang, Central Java, Indonesia. *Atmosphere, 13*, 1092. https://ui.adsabs.harvard.edu/abs/2022Atmos..13.1092H

Hmiel, B., Petrenko, V. V., Dyonisius, M. N., Buizert, C., Smith, A. M., Place, P. F., et al. (2020). Preindustrial 14CH4 indicates greater anthropogenic fossil CH4 emissions. *Nature, 578*(7795), 409-412. https://doi.org/10.1038/s41586-020-1991-8

Hodson, E. L., Poulter, B., Zimmermann, N. E., Prigent, C., & Kaplan, J. O. (2011). The El Niño–Southern Oscillation and wetland methane interannual variability. *Geophysical Research Letters, 38*(8). https://agupubs.onlinelibrary.wiley.com/doi/abs/10.1029/2011GL046861

Jain, M. C., Kumar, S., Wassmann, R., Mitra, S., Singh, S. D., Singh, J. P., et al. (2000). Methane Emissions from Irrigated Rice Fields in Northern India (New Delhi). *Nutrient Cycling in Agroecosystems, 58*(1), 75-83. https://doi.org/10.1023/A:1009882216720

Janardanan, R., Maksyutov, S., Tsuruta, A., Wang, F., Tiwari, Y. K., Valsala, V., et al. (2020). Country-Scale Analysis of Methane Emissions with a High-Resolution Inverse Model Using GOSAT and Surface Observations. *Remote Sensing, 12*(3), 375. https://www.mdpi.com/2072-4292/12/3/375

Janssens-Maenhout, G., Crippa, M., Guizzardi, D., Muntean, M., Schaaf, E., Dentener, F., et al. (2019). EDGAR v4.3.2 Global Atlas of the three major greenhouse gas emissions for the period 1970–2012. *Earth Syst. Sci. Data, 11*(3), 959-1002. https://essd.copernicus.org/articles/11/959/2019/

Kuze, A., Suto, H., Nakajima, M., & Hamazaki, T. (2009). Thermal and near infrared sensor for carbon observation Fourier-transform spectrometer on the Greenhouse Gases Observing Satellite for greenhouse gases monitoring. *Applied Optics, 48*(35), 6716-6733. http://opg.optica.org/ao/abstract.cfm?URI=ao-48-35-6716

Kuze, A., Suto, H., Shiomi, K., Kawakami, S., Tanaka, M., Ueda, Y., et al. (2016). Update on GOSAT TANSO-FTS performance, operations, and data products after more than 6 years

in space. *Atmos. Meas. Tech., 9*(6), 2445-2461. https://amt.copernicus.org/articles/9/2445/2016/
Lan, X., Basu, S., Schwietzke, S., Bruhwiler, L. M. P., Dlugokencky, E. J., Michel, S. E., et al. (2021a). Improved Constraints on Global Methane Emissions and Sinks Using δ13C-CH4. *Global Biogeochemical Cycles, 35*(6), e2021GB007000. https://agupubs.onlinelibrary.wiley.com/doi/abs/10.1029/2021GB007000
Lan, X., Nisbet, E. G., Dlugokencky, E. J., & Michel, S. E. (2021b). What do we know about the global methane budget? Results from four decades of atmospheric CH4 observations and the way forward. *Philosophical Transactions of the Royal Society A: Mathematical, Physical and Engineering Sciences, 379*(2210), 20200440. https://royalsocietypublishing.org/doi/abs/10.1098/rsta.2020.0440
Laughner, J. L., Neu, J. L., Schimel, D., Wennberg, P. O., Barsanti, K., Bowman, K. W., et al. (2021). Societal shifts due to COVID-19 reveal large-scale complexities and feedbacks between atmospheric chemistry and climate change. *Proceedings of the National Academy of Sciences, 118*(46), e2109481118. https://www.pnas.org/doi/abs/10.1073/pnas.2109481118
Lu, X., Jacob, D. J., Zhang, Y., Maasakkers, J. D., Sulprizio, M. P., Shen, L., et al. (2021). Global methane budget and trend, 2010–2017: complementarity of inverse analyses using in situ (GLOBALVIEWplus CH4 ObsPack) and satellite (GOSAT) observations. *Atmos. Chem. Phys., 21*(6), 4637-4657. https://acp.copernicus.org/articles/21/4637/2021/
Lunt, M. F., Palmer, P. I., Lorente, A., Borsdorff, T., Landgraf, J., Parker, R. J., & Boesch, H. (2021). Rain-fed pulses of methane from East Africa during 2018–2019 contributed to atmospheric growth rate. *Environmental Research Letters, 16*(2), 024021. http://dx.doi.org/10.1088/1748-9326/abd8fa
Ma, S., Worden, J. R., Bloom, A. A., Zhang, Y., Poulter, B., Cusworth, D. H., et al. (2021). Satellite Constraints on the Latitudinal Distribution and Temperature Sensitivity of Wetland Methane Emissions. *AGU Advances, 2*(3), e2021AV000408. https://agupubs.onlinelibrary.wiley.com/doi/abs/10.1029/2021AV000408
Ma, S., Bloom, A.A., Watts, J.D., Quetin, G.R., Donatella, Z., Euskirchen, E.S., et al. (2023). Resolving the Carbon-Climate Feedback Potential of Wetland CO2 and CH4 Fluxes in Alaska. *Global Biogeochemical Cycles*, 37(9), p.e2022GB007524 https://agupubs.onlinelibrary.wiley.com/doi/abs/10.1029/2022GB007524
Maasakkers, J. D., Jacob, D. J., Sulprizio, M. P., Turner, A. J., Weitz, M., Wirth, T., et al. (2016). Gridded National Inventory of U.S. Methane Emissions. *Environmental Science & Technology, 50*(23), 13123-13133. https://doi.org/10.1021/acs.est.6b02878
Maasakkers, J. D., Jacob, D. J., Sulprizio, M. P., Scarpelli, T. R., Nesser, H., Sheng, J. X., et al. (2019). Global distribution of methane emissions, emission trends, and OH concentrations and trends inferred from an inversion of GOSAT satellite data for 2010–2015. *Atmos. Chem. Phys., 19*(11), 7859-7881. https://acp.copernicus.org/articles/19/7859/2019/
Monteil, G., Houweling, S., Butz, A., Guerlet, S., Schepers, D., Hasekamp, O., et al. (2013). Comparison of CH4 inversions based on 15 months of GOSAT and SCIAMACHY observations. *Journal of Geophysical Research: Atmospheres, 118*(20), 11,807-811,823. https://agupubs.onlinelibrary.wiley.com/doi/abs/10.1002/2013JD019760
Murguia-Flores, F., Arndt, S., Ganesan, A. L., Murray-Tortarolo, G., & Hornibrook, E. R. C. (2018). Soil Methanotrophy Model (MeMo v1.0): a process-based model to quantify global uptake of atmospheric methane by soil. *Geosci. Model Dev., 11*(6), 2009-2032. https://gmd.copernicus.org/articles/11/2009/2018/
Murray, L. T., Jacob, D. J., Logan, J. A., Hudman, R. C., & Koshak, W. J. (2012). Optimized regional and interannual variability of lightning in a global chemical transport model

constrained by LIS/OTD satellite data. *Journal of Geophysical Research: Atmospheres, 117*(D20). https://agupubs.onlinelibrary.wiley.com/doi/abs/10.1029/2012JD017934

Nisbet, E. G., Dlugokencky, E. J., Manning, M. R., Lowry, D., Fisher, R. E., France, J. L., et al. (2016). Rising atmospheric methane: 2007–2014 growth and isotopic shift. *Global Biogeochemical Cycles, 30*(9), 1356-1370. https://agupubs.onlinelibrary.wiley.com/doi/abs/10.1002/2016GB005406

Nisbet, E. G., Manning, M. R., Dlugokencky, E. J., Fisher, R. E., Lowry, D., Michel, S. E., et al. (2019). Very Strong Atmospheric Methane Growth in the 4 Years 2014–2017: Implications for the Paris Agreement. *Global Biogeochemical Cycles, 33*(3), 318-342. https://agupubs.onlinelibrary.wiley.com/doi/abs/10.1029/2018GB006009

NOAA (2023). Global CH4 Monthly Means, available at: https://gml.noaa.gov/ccgg/trends_ch4/, last access, Nov 19, 2023.

Oh, Y., Zhuang, Q., Welp, L. R., Liu, L., Lan, X., Basu, S., et al. (2022). Improved global wetland carbon isotopic signatures support post-2006 microbial methane emission increase. *Communications Earth & Environment, 3*(1), 159. https://doi.org/10.1038/s43247-022-00488-5

Pandey, S., Houweling, S., Krol, M., Aben, I., Chevallier, F., Dlugokencky, E. J., et al. (2016). Inverse modeling of GOSAT-retrieved ratios of total column CH4 and CO2 for 2009 and 2010. *Atmos. Chem. Phys., 16*(8), 5043-5062. https://acp.copernicus.org/articles/16/5043/2016/

Parker, R. J., Webb, A., Boesch, H., Somkuti, P., Barrio Guillo, R., Di Noia, A., et al. (2020). A decade of GOSAT Proxy satellite CH4 observations. *Earth Syst. Sci. Data, 12*(4), 3383-3412. https://essd.copernicus.org/articles/12/3383/2020/

Parker, R. J. & Boesch, H. (2020). University of Leicester GOSAT Proxy XCH4 v9.0. Centre for Environmental Data Analysis, 07 May 2020. https://dx.doi.org/10.5285/18ef8247f52a4cb6a14013f8235cc1eb

Peng, S., Lin, X., Thompson, R. L., Xi, Y., Liu, G., Hauglustaine, D., et al. (2022). Wetland emission and atmospheric sink changes explain methane growth in 2020. *Nature, 612*(7940), 477-482. https://doi.org/10.1038/s41586-022-05447-w

Prather, M. J., Holmes, C. D., & Hsu, J. (2012). Reactive greenhouse gas scenarios: Systematic exploration of uncertainties and the role of atmospheric chemistry. *Geophysical Research Letters, 39*(9). https://agupubs.onlinelibrary.wiley.com/doi/abs/10.1029/2012GL051440

Putnam, A. E. and Broecker, W. S. (2017). Human-induced changes in the distribution of rainfall. *Sci. Adv., 3*, e160087. https://doi.org/10.1126/sciadv.1600871

Qu, Z., Jacob, D. J., Shen, L., Lu, X., Zhang, Y., Scarpelli, T. R., et al. (2021). Global distribution of methane emissions: a comparative inverse analysis of observations from the TROPOMI and GOSAT satellite instruments. *Atmos. Chem. Phys., 21*(18), 14159-14175. https://acp.copernicus.org/articles/21/14159/2021/

Qu, Z., Jacob, D. J., Zhang, Y., Shen, L., Varon, D. J., Lu, X., et al. (2022). Attribution of the 2020 surge in atmospheric methane by inverse analysis of GOSAT observations. *Environmental Research Letters, 17*(9), 094003. https://dx.doi.org/10.1088/1748-9326/ac8754

Reliefweb (2020). India: Floods and landslides, available at: https://reliefweb.int/disaster/fl-2020-000164-ind, last access: Nov 19, 2023.

Rigby, M., Montzka, S. A., Prinn, R. G., White, J. W. C., Young, D., O'Doherty, S., et al. (2017). Role of atmospheric oxidation in recent methane growth. *Proceedings of the National Academy of Sciences, 114*(21), 5373-5377. https://www.pnas.org/doi/abs/10.1073/pnas.1616426114

Rodgers, C. D. (2000). *Inverse Methods for Atmospheric Sounding*.

Saunois, M., Stavert, A. R., Poulter, B., Bousquet, P., Canadell, J. G., Jackson, R. B., et al. (2020). The Global Methane Budget 2000–2017. *Earth Syst. Sci. Data, 12*(3), 1561-1623. https://essd.copernicus.org/articles/12/1561/2020/

Save, H., Bettadpur, S., & Tapley, B. D. (2016). High-resolution CSR GRACE RL05 mascons. *Journal of Geophysical Research: Solid Earth, 121*(10), 7547-7569. https://agupubs.onlinelibrary.wiley.com/doi/abs/10.1002/2016JB013007

Save, H. (2020). CSR GRACE and GRACE-FO RL06 Mascon Soluitons v02, https:dx.doi.org/10.15781/cgq9-nh24.

Scarpelli, T. R., Jacob, D. J., Grossman, S., Lu, X., Qu, Z., Sulprizio, M. P., et al. (2022). Updated Global Fuel Exploitation Inventory (GFEI) for methane emissions from the oil, gas, and coal sectors: evaluation with inversions of atmospheric methane observations. *Atmos. Chem. Phys., 22*(5), 3235-3249. https://acp.copernicus.org/articles/22/3235/2022/

Schaefer, H., Fletcher, S. E. M., Veidt, C., Lassey, K. R., Brailsford, G. W., Bromley, T. M., et al. (2016). A 21st-century shift from fossil-fuel to biogenic methane emissions indicated by 13CH4. *Science, 352*(6281), 80-84. https://www.science.org/doi/abs/10.1126/science.aad2705

Stanevich, I., Jones, D. B. A., Strong, K., Keller, M., Henze, D. K., Parker, R. J., et al. (2021). Characterizing model errors in chemical transport modeling of methane: using GOSAT XCH4 data with weak-constraint four-dimensional variational data assimilation. *Atmos. Chem. Phys., 21*(12), 9545-9572. https://acp.copernicus.org/articles/21/9545/2021/

Statista (2023). Amount of rainfall measured across India from 2012 to 2021, available at: https://www.statista.com/statistics/834443/india-annual-rainfall-volume/, last access: Nov 19, 2023.

Stevenson, D. S., Derwent, R. G., Wild, O., & Collins, W. J. (2022). COVID-19 lockdown emission reductions have the potential to explain over half of the coincident increase in global atmospheric methane. *Atmos. Chem. Phys., 22*(21), 14243-14252. https://acp.copernicus.org/articles/22/14243/2022/

Szopa, S., Naik, V., Adhikary, B., Artaxo, P., Berntsen, T., Collins, W. D., et al. (Eds.). (2021). *Short-Lived Climate Forcers. In Climate Change 2021: The Physical Science Basis. Contribution of Working Group I to the Sixth Assessment Report of the Intergovernmental Panel on Climate Change*. Cambridge, United Kingdom and New York, NY, USA: Cambridge University Press.

Turner, A. J., Frankenberg, C., Wennberg, P. O., & Jacob, D. J. (2017). Ambiguity in the causes for decadal trends in atmospheric methane and hydroxyl. *Proceedings of the National Academy of Sciences, 114*(21), 5367-5372. https://www.pnas.org/doi/abs/10.1073/pnas.1616020114

USDA (2023). Pakistan rice area, yield, and production, available at: https://ipad.fas.usda.gov/countrysummary/Default.aspx?id=PK&crop=Rice, last access: Nov 19, 2023.

van der Werf, G. R., Randerson, J. T., Giglio, L., van Leeuwen, T. T., Chen, Y., Rogers, B. M., et al. (2017). Global fire emissions estimates during 1997–2016. *Earth Syst. Sci. Data, 9*(2), 697-720. https://essd.copernicus.org/articles/9/697/2017/

Wang, X., Jacob, D. J., Eastham, S. D., Sulprizio, M. P., Zhu, L., Chen, Q., et al. (2019). The role of chlorine in global tropospheric chemistry. *Atmos. Chem. Phys., 19*(6), 3981-4003. https://acp.copernicus.org/articles/19/3981/2019/

Wecht, K. J., Jacob, D. J., Frankenberg, C., Jiang, Z., & Blake, D. R. (2014). Mapping of North American methane emissions with high spatial resolution by inversion of SCIAMACHY satellite data. *Journal of Geophysical Research: Atmospheres, 119*(12), 7741-7756. https://agupubs.onlinelibrary.wiley.com/doi/abs/10.1002/2014JD021551

World Bank (2023a) Indonesia Average Precipitation, available at https://tradingeconomics.com/indonesia/precipitation, last access: Nov 19, 2023.

World Bank (2023b) Papua New Guinea Average Precipitation, available at https://tradingeconomics.com/papua-new-guinea/precipitation, last access: Nov 19, 2023.

Worden, J. R., Bloom, A. A., Pandey, S., Jiang, Z., Worden, H. M., Walker, T. W., et al. (2017). Reduced biomass burning emissions reconcile conflicting estimates of the post-2006 atmospheric methane budget. *Nature Communications, 8*(1), 2227. https://doi.org/10.1038/s41467-017-02246-0

Worden, J. R., Pandey, S., Zhang, Y., Cusworth, D. H., Qu, Z., Bloom, A. A., et al. (2023). Verifying Methane Inventories and Trends With Atmospheric Methane Data. *AGU Advances, 4*(4), e2023AV000871. https://agupubs.onlinelibrary.wiley.com/doi/abs/10.1029/2023AV000871

Yin, Y., Chevallier, F., Ciais, P., Bousquet, P., Saunois, M., Zheng, B., et al. (2021). Accelerating methane growth rate from 2010 to 2017: leading contributions from the tropics and East Asia. *Atmos. Chem. Phys., 21*(16), 12631-12647. https://acp.copernicus.org/articles/21/12631/2021/

Zhang, Y. and Fueglistaler, S. (2019). Mechanism for increasing tropical rainfall unevenness with global warming. *Geophysical Research Letters, 46, 14836-14843*. https://agupubs.onlinelibrary.wiley.com/doi/abs/10.1029/2019GL086058

Zhang, B., Tian, H., Ren, W., Tao, B., Lu, C., Yang, J., et al. (2016). Methane emissions from global rice fields: Magnitude, spatiotemporal patterns, and environmental controls. *Global Biogeochemical Cycles, 30*(9), 1246-1263. https://agupubs.onlinelibrary.wiley.com/doi/abs/10.1002/2016GB005381

Zhang, Y., Jacob, D. J., Lu, X., Maasakkers, J. D., Scarpelli, T. R., Sheng, J. X., et al. (2021). Attribution of the accelerating increase in atmospheric methane during 2010–2018 by inverse analysis of GOSAT observations. *Atmos. Chem. Phys., 21*(5), 3643-3666. https://acp.copernicus.org/articles/21/3643/2021/

Zhang, Y., Fang, S., Chen, J., Lin, Y., Chen, Y., Liang, R., et al. (2022). Observed changes in China's methane emissions linked to policy drivers. *Proceedings of the National Academy of Sciences, 119*(41), e2202742119. https://www.pnas.org/doi/abs/10.1073/pnas.2202742119

Zhang, Z., Zimmermann, N. E., Calle, L., Hurtt, G., Chatterjee, A., & Poulter, B. (2018). Enhanced response of global wetland methane emissions to the 2015–2016 El Niño-Southern Oscillation event. *Environmental Research Letters, 13*(7), 074009. https://dx.doi.org/10.1088/1748-9326/aac939

Zhang, Z., Poulter, B., Feldman, A. F., Ying, Q., Ciais, P., Peng, S., & Li, X. (2023). Recent intensification of wetland methane feedback. *Nature Climate Change, 13*(5), 430-433. https://doi.org/10.1038/s41558-023-01629-0

Zhu, Q., Peng, C., Ciais, P., Jiang, H., Liu, J., Bousquet, P., et al. (2017). Interannual variation in methane emissions from tropical wetlands triggered by repeated El Niño Southern Oscillation. *Glob Chang Biol, 23*(11), 4706-4716.

Acknowledgments

Funding: Z.Q. acknowledges startup funding from the College of Sciences at North Carolina State University. Work at Harvard was supported by the NASA Carbon Monitoring System. R.J.P. is funded via the UK National Centre for Earth Observation (NE/W004895/1). We thank the Japanese Aerospace Exploration Agency, National Institute for Environmental Studies, and the Ministry of Environment for the GOSAT data and their continuous support as part of the Joint Research

Agreement. This research used the ALICE High Performance Computing Facility at the University of Leicester for the GOSAT retrievals. Part of this research was carried out at the Jet Propulsion Laboratory, California Institute of Technology, under a contract with the National Aeronautics and Space Administration (80NM0018D0004).

Author contributions: Z.Q. and D.J.J. designed the project; Z.Q. performed the inversion simulation and interpreted results in consultation with D.J.J.; Z.Q. led the writing with inputs from D.J.J, A.B., J.W., R.J.P., and H.B.; A.B. processed the GRACE and GRACE/FO data; R.J.P. and H.B. provided GOSAT data and assisted in its interpretation.

Competing interests: Authors declare that they have no competing interests.

Data and materials availability: The GOSAT methane retrieval is available at https://www.leos.le.ac.uk/data/GHG/GOSAT/v9.0/CH4_GOS_OCPR_v9.0_final_nceo_2009_2022.tar.gz (last accessed Nov 19, 2023). The data that support the findings of this study are openly available at the following URL/DOI: https://doi.org/10.5285/18ef8247f52a4cb6a14013f8235cc1eb. The GRACE and GRACE/FO Mascon data (version RL06.2) product was downloaded from http://www2.csr.utexas.edu/grace (last access Dec 1, 2023). All data are available in the main text or the supplementary materials.